SCIENCE CHINA
Chemistry

•INVITED REVIEWS•

October 2019 Vol.62 No.10: 1286–1299
https://doi.org/10.1007/s11426-019-9519-9

Designing solid-state interfaces on lithium-metal anodes: a review

Chen-Zi Zhao[1], Hui Duan[2,4], Jia-Qi Huang[3], Juan Zhang[2], Qiang Zhang[1*], Yu-Guo Guo[2,4*] & Li-Jun Wan[2,4]

[1]*Beijing Key Laboratory of Green Chemical Reaction Engineering and Technology, Department of Chemical Engineering, Tsinghua University, Beijing 100084, China;*
[2]*CAS Key Laboratory of Molecular Nanostructure and Nanotechnology, CAS Research/Education Center for Excellence in Molecular Sciences, Beijing National Laboratory for Molecular Sciences, Institute of Chemistry, Chinese Academy of Sciences, Beijing 100190, China;*
[3]*Advanced Research Institute of Multidisciplinary Science, Beijing Institute of Technology, Beijing 100081, China;*
[4]*University of Chinese Academy of Sciences, Beijing 100049, China*

Received April 14, 2019; accepted June 19, 2019; published online September 9, 2019

Li-metal anodes are one of the most promising energy storage systems that can considerably exceed the current technology to meet the ever-increasing demand of power applications. The apparent cycling performances and dendrite challenges of Li-metal anodes are highly influenced by the interface layer on the Li-metal anode because the intrinsic high reactivity of metallic Li results in an inevitable solid-state interface layer between the Li-metal and electrolytes. In this review, we summarize the recent progress on the interfacial chemistry regarding the interactions between electrolytes and ion migration through dynamic interfaces. The critical factors that affect the interface formation for constructing a stable interface with a low resistance are reviewed. Moreover, we review emerging strategies for rationally designing multiple-structured solid-state electrolytes and their interfaces, including the interfacial properties within hybrid electrolytes and the solid electrolyte/electrode interface. Finally, we present scientific issues and perspectives associated with Li-metal anode interfaces toward a practical Li-metal battery.

lithium-metal anode, solid-state electrolyte, energy chemistry, rechargeable lithium-metal batteries, solid electrolyte/electrode interface

Citation: Zhao CZ, Duan H, Huang JQ, Zhang J, Zhang Q, Guo YG, Wan LJ. Designing solid-state interfaces on lithium-metal anodes: a review. *Sci China Chem*, 2019, 62: 1286–1299, https://doi.org/10.1007/s11426-019-9519-9

1 Introduction

Next-generation rechargeable batteries have increased the use of portable devices and even transportation. They have transformed modern society and will continue to play a crucial role in the future. In recent decades, Li-ion batteries have achieved spectacular success and dominate the present energy storage market of electronic gadgets. The significant efforts devoted toward rocking chair Li-ion batteries have pushed their energy density to the limit. However, the booming demand for mobile power sources, such as cell phones and electric vehicles, requires exploration of new systems and chemistry beyond the horizon of Li-ion batteries. To achieve the high energy density that exceeds that of current technology, changing from Li-ion to Li-metal batteries is a particularly promising idea as metallic Li stores much more charge than graphite anodes.

Rechargeable Li-metal anodes afford an extremely high theoretical specific capacity of 3,860 mA h g^{-1}, which is ten times higher than that of current commercial graphite anodes, and they have the most negative electrochemical potential of −3.040 V versus a standard hydrogen electrode, offering tremendous opportunities for high-voltage batteries.

*Corresponding authors (email: zhang-qiang@mails.tsinghua.edu.cn; ygguo@iccas.ac.cn)

However, the high reactivity of metallic Li not only enables an attractive energy density but also results in inevitable interfacial reactions on the anode surface in a practical battery. Actually, the investigation of Li-metal batteries dates back to the 1960s; however, the dendritic Li deposition morphology and the unsatisfying cycle efficiency resulting from the unstable interface have significantly hindered the application of Li-metal batteries [1]. Both Li-ion migration and reduction are strongly dependent on the interfacial layer, constituting the initial stages of Li-metal deposition and largely determining the cycle performances.

In the most widely used configurations, the Li-metal anode is exposed to nonaqueous Li-conducting electrolytes and faces the cathode through a separator for the electrochemical reactions [2]. The severe reactions of Li-metal and electrolytes bring about anode corrosion and electrolyte consumption. Hence, dendrites form and the battery lifespan are considerably shortened, especially in pouch cells [3,4]. Batteries utilizing organic liquid electrolytes also suffer from flammability and potential leakage risks. Recently, the replacement of organic liquid electrolytes by solid-state electrolytes has offered opportunities to construct batteries that are quite safe [5–7]. Nevertheless, new interfaces appear in solid-state Li-metal batteries and insufficient solid contacts considerably retard ion transportation. Moreover, this represents a serious obstacle for further processes because there is a lack of knowledge regarding the reactions and processes on the interface [8,9].

In this contribution, recent advances on the interfacial chemistry and interface design strategy for Li-metal anodes are reviewed. First, we discuss the basic principles of interface formation and ion conduction properties of the solid-electrolyte interphase in nonaqueous batteries. Accordingly, the approaches for a stable interface construction are presented. Then, interfacial engineering strategies for solid-state Li-metal batteries are reviewed, providing more understanding about the energy chemistry underpinning these complex battery systems. Finally, a general conclusion and perspectives on the solid-state interface design on Li-metal anodes are presented for further directions.

2 Understandings of the interfacial chemistry

2.1 Ionic and electronic conduction at interfaces

Interfaces on Li-metal anodes are essential to understand because they are inevitable and play a key role in practical batteries. The negative equilibrium potential of Li-metal not only renders a high-energy density but also results in high chemical activity, generating various interfaces through electrochemical reactions between Li-metal anodes and electrolytes; the situation is even more challenging when structured metal anodes with large surfaces or solid-liquid hybrid electrolytes are employed [10–12].

The interfaces on Li-metal anodes are generally regarded as a solid-electrolyte interphase (SEI), which is ideal for conducting Li-ions and electronic insulation to prevent side reactions [13,14]. Generally, cell failure is triggered by the SEI instability, constituting an indicator of battery failure. The SEI is continuously renewed in charge-discharge processes. *In situ* and operando technologies have provided opportunities to perform electrochemical measurements during battery operations [15]. Cui and co-workers [16] observed SEI nanostructures formed in different electrolytes by cryo-electron microscopy, where Li-metal dendrite growth may change their direction at the kinks. Bieker *et al*. [17] studied the ongoing Li corrosion rate and the passivating quality of the SEI. They also provided a general model of the different stages. *In situ* micro-FTIR spectroscopy has also been employed to investigate the interface layer between Li-metal and polyethylene oxide (PEO)-based polymer electrolytes [18] to detect the reduction reactions of oxygen and water. Sacci *et al*. [19] utilized *in situ* electrochemical scanning transmission electron microscopy (ec-S/TEM) to track Li nucleation and the growth mechanism in carbonate-based electrolytes. They revealed that SEI is approximately twice as dense as the electrolyte, which is determined using imaging and electron scattering theory, and they observed site-specific locations for Li nucleation and growth. The structure and components of the SEI have been investigated over the past 30 years, where multilayer models and mosaic models are established and experimentally confirmed [20–25]. However, the intricate reactions and ion transportations still remain a mystery. Recently, new insights have been proposed. Cheng *et al*. [26] proposed that a mixed conducting interphase (MCI) coexists in working batteries to migrate both electrons and Li-ions, which was also verified by Maier [27].

The MCI layer can act as a transition state of the SEI or an inner layer of a stable interfacial film, improving ionic conduction (Figure 1(a)). During the initial stages of the interfacial reactions, an ultrathin film is favorable for electron tunneling. The growth stops at a certain tunneling threshold to form an electron insulator layer. Consequently, the MCI acts an intermediate. However, not all interfacial reactions result in an electron insulator layer; the Li-metal-$Li_{10}GeP_2S_{12}$ interface contains the Li-Ge alloy, Li_2S, Li_3P, and others, some of which can migrate electrons in continuous reactions, and the MCI layer keeps growing [28]. In another case, the MCI constitutes an inner electronic channel of the interface layer, where components in the outer layer, such as organic complexes, block electrons for the side reactions. This electric conduction inner layer can temporarily reserve Li-ions at grain boundary regions, accelerating Li-ion transportation and buffering the concentration gradient. Furthermore, when a host is employed for a uniform plating/

striping process and the tolerating volume changes, the ionic and electronic channels are interconnected on the nanoscale or microscale for structured Li-metal anodes, where the electronic channels are usually provided by a conducting framework [29,30].

The roles of the MCI can be verified and experimentally reconstructed in Li-metal batteries. Yan *et al*. [31] introduced Cu atoms into the original interfacial layer to form a mosaic MCI layer (Figure 1(b)). Compared with a lithium fluoride (LiF)-rich SEI layer, the mosaic mixed LiF/Cu conducting interphase rendered enhanced Li diffusion and storage at the grain boundaries, which can be simply realized via a controllable displacement reaction of the Li metal anode and cupric fluoride (CuF_2). This armored MCI layer containing Li_3N, LiF, LiN_xO_y, and Cu is able to reserve Li ions prior to metallic Li anodes with Cu atoms destroying the ordered crystals and regulating the uniform deposition of Li-metal. The high surface energy and high Young's modulus also contribute to the uniform metal anodes even at a high current density. Hence, the MCI on a Li-metal anode deserves more understanding, and a better fabrication strategy is needed to achieve a practical Li-metal battery.

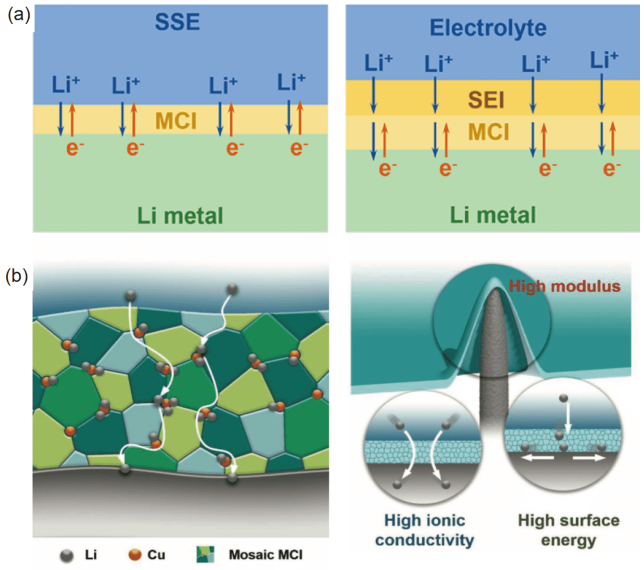

Figure 1 MCI in the interfacial film of a Li-metal and electrolyte. (a) MCI between the Li metal and SSE (left) and MCI as an inner layer between the SEI and Li metal (right) [26]. (b) Schematic diagram of an armored MCI and its functions on Li plating. Left: The introduction of Cu atoms improves the ionic conductivity of the LiF/Cu-based MCI film by providing more diffusion domains and the Li storage at the grain boundary regions of LiF/Cu compared to the poor ionic conductivity of the LiF-rich SEI film; right: Armored MCI possesses a high surface energy to achieve a uniform Li-ion distribution, high ionic conductivity to render rapid Li-ion diffusion, and high Young's modulus to suppress the growth of Li dendrites [31] (color online).

2.2 Interfacial reactions induced by ion-solvent complexes

An interfacial layer, as an essential part that determines the performances in Li-metal batteries, is formed from the interfacial reaction and is considerably associated with the solvation structure. For nonaqueous electrolytes, both solvents and ions are usually coordinated to form solvated ions. In particular, Li ions and their solvation sheath diffuse together through separator and touch the Li metal anode surface in Li metal batteries [32]. Then, the solvation sheath is reduced to constitute the components in the interfacial layer [32]. To provide a deeper understanding, the mechanisms of the interfacial reactions have been carefully investigated.

It has been experimentally observed that electrolytes with both solvents and salts usually decompose much more violently than their pure solvent counterparts, especially in alkaline-metal batteries. The recent development of advanced theoretical calculations has provided abundant fundamental understanding about the chemistry inside a complicated battery. Recent calculation methods include first-principles computational methods, *ab initio* molecular dynamics (AIMD) simulations, and thermodynamic calculations enabled by materials databases [33]. The interfacial reactions induced by ions and solvents have been revealed by first-principles calculations and molecular dynamics simulations. Chen *et al*. [34] employed sodium-propylene carbonate (Na^+-PC) solution as a model system. The ion-solvent complex has a much lower lowest unoccupied molecular orbital (LUMO) that contributes to the reduction of electrolytes and interfacial layer formation. Once the PC molecule coordinated with Na^+ to form a $[NaPC]^+$ complex, the LUMO level decreased from −0.17 (considering the solvent effects) to −5.28 eV (Figure 2(a)). This huge difference resulted in the weakened thermodynamic stability of the solvents and even triggered gas evolution [35], which can be attributed to the orbital hybridization, as verified by *in situ* optical microscopic observations. Additionally, the kinetics of the reduction reaction were simulated by AIMD and showed that solvated ions are indispensable in C–O bond breaking. Moreover, metallic Li electrodes and the corresponding electrolytes render similar features as in the sodium system. The ion-solvent complexes provide a deeper understanding of the interfacial reactions on metal anodes.

Furthermore, to investigate the contribution of ion-solvent complexes to interfacial reactions, various metal ions, including Li^+, Na^+, K^+, Mg^{2+}, and Ca^{2+}, were used to interact with multiple electrolytes, including most of the typical ester and ether electrolyte systems (Figure 2(b)) [36]. Generally, the LUMO energy of the involved ion-solvent complexes is lower than that of corresponding pure solvents according to first-principles calculations, which produces a higher interfacial reactivity. This phenomenon is more notable for cations in ether-based electrolytes with a greater LUMO difference that can be as large as −9.46 eV. For ester solvents, the LUMO energy levels and binding energy follow a good

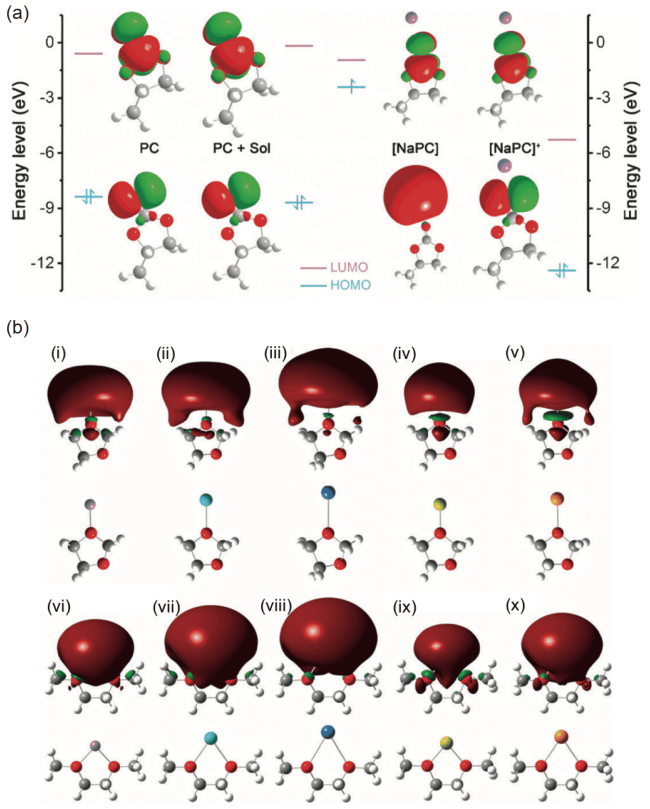

Figure 2 Analysis of ion-solvent complexes. (a) Frontier molecular orbital theory analysis. Frontier molecular orbital levels of PC (single PC molecule), PC+Sol (PC molecule with solvent effects considered), [NaPC] (Na-atom-PC complex) and $[NaPC]^+$ (Na^+-ion-PC complex). The red and green regions represent the positive and negative parts of the LUMO and HOMO wave functions, respectively (isovalue: 0.02). The hydrogen, lithium, carbon, and oxygen atoms are marked with white, purple, gray, and red, respectively [34]. (b) The visual LUMOs and corresponding optimized geometrical structures of ion-solvent complexes. (i) Li^+-DOL; (ii) Na^+-1,3-dioxolane (DOL); (iii) K^+-DOL; (iv) Mg^{2+}-DOL; (v) Ca^{2+}-DOL; (vi) Li^+-1,2-dimethoxyethane (DME); (vii) Na^+-DME; (viii) K^+-DME; (ix) Mg^{2+}-DME; (x) Ca^{2+}-DME. H white, Li purple, C gray, O red, Na green, Mg blue, K yellow, Ca orange. The red and green regions of LUMOs represent the positive and negative parts of orbitals, respectively [36] (color online).

linear relationship. The metal ions adjust the carbon 2p orbital contribution in the LUMO of the complexes in ester electrolytes, thus decreasing the LUMO energy level. However, the situation is more complicated for ether electrolytes. The binding energy and C–O bond length of ion-ether complexes are transformed significantly as well as the metal atomic orbitals, causing a reduced stability and severe interfacial reactions.

Moreover, not only cation-solvent complexes but also cation–anion and solvent-solvent complexes exhibit solvation effects, where the binding energy is reduced and the dissolution behaviors of Li salts can be predicted [37]. A breakthrough based on this concept is the dissolution of $LiNO_3$ in carbonate-based electrolyte with an extended voltage window. $LiNO_3$ is favorable for constructing a stable interfacial layer on Li-metal anodes and has been employed widely in ether-based electrolytes. However, its poor solubility in carbonate electrolytes restricts its application in high-voltage batteries, which is of vital importance to achieve a high energy density. To address this problem, Yan *et al*. [38] achieved a high solubility of $LiNO_3$ without the destruction in an ethylene carbonate (EC)/diethyl carbonate (DEC) mixture under room temperature by adding only a trace amount of copper fluoride (CuF_2). In routine EC/DEC electrolytes, nuclear magnetic resonance (NMR) spectra indicated that electron-donated NO_3^- strongly interacts with Li-ions, inducing a shielding effect. However, the shielding effect in the $LiNO_3/CuF_2$ electrolyte can be considerably weakened owing to the coordination of Cu^{2+} and EC/DEC molecules, where Cu^{2+} carries more charge but possesses a similar ionic radius as Li^+. Molecular dynamics (MD) simulations also suggest that NO_3^- can coordinate with copper ions and the Cu^{2+}-NO_3^- interactions are stronger than the Li^+-NO_3^- interactions, revealing the mechanism for increased solubility. Consequently, batteries employing a high-voltage $LiNi_{0.80}Co_{0.15}Al_{0.05}O_2$ (NCA) cathode and a Li metal anode with dissolved $LiNO_3$ in ester electrolytes achieve a high average Coulombic efficiency (>99.5%) at 0.5 C.

Therefore, by determining the role of ion-solvent complexes, it is possible to regulate interfacial reactions by alternating the ion solvation sheath, which affects the components of the interfacial layer and the battery performance.

3 Constructing an interfacial layer in nonaqueous batteries

3.1 Artificial interface layer

Constructing an artificial layer on a metallic anode is one of the most direct and effective ways to achieve a stable interface under battery operations. The *ex situ*-formed interfacial layer can regulate the ion distribution prior to the reduction process on the metal surface and serve as a protective layer during repeated cycling [39].

Adjusting the components of the artificial layer determines the initial Li deposition morphology, producing uniform and even columnar Li metal anodes. To alter the routine heterogeneous interfacial layer, Zhang and co-workers [40] coated an artificial LiF-rich layer on a primary copper current collector by nonaqueous lithium hexafluorophosphate ($LiPF_6$) solution immersion. This uniform LiF layer exhibited weak adsorption of Li^+ compared to the bare Cu current collector, thus inducing efficient Li diffusion channels. Li ions were deposited and diffused rapidly with a low energy barrier during charging and then grew horizontally to the corresponding nucleation sites under spatial confinement to finally form a columnar morphology with low interfacial resistances. Moreover, columnar Li-metal electrodes can also be produced by nanodiamond additives that are co-

deposited with Li-ions, enhancing the Coulombic efficiency of metal anodes [41].

Rechargeable Li metal batteries require the repeated plating and stripping of metallic anodes. Various strategies have been proposed to synthesize an artificial layer for dendrite growth inhibition and enhanced interface stability. Recently, Wang and co-workers [42] designed an interface from reactive polymers instead of from reactive organic electrolytes. The composite interface layer, which included graphene oxide, LiF nanoparticles, and polymeric Li salts, exhibited attractive mechanical properties and passivation properties, which enabled stable cycling with lean electrolytes. An organic-inorganic composite interfacial film can also be produced by *in situ* synthesis of a Si-interlinked OOCOR layer for a LiCl host [43].

To offer effective protection under huge volumetric changes and to maintain a high ionic conductivity, Huang and co-workers [44] hybridized poly(vinylidene-*co*-hexafluoropropylene) (PVDF-HFP) and LiF particles to synthesize a 12-μm-thick composite film that had superb shape compliance, an ultrahigh Young's modulus, and a favorable ion transportation ability (Figure 3(a)). The PVDF-HFP matrix acts as the soft part for excellent adhesion, and LiF particles contribute to the uniform Li deposition for a prolonged lifespan. Furthermore, Archer and co-workers [45] proposed in-built fast transport via 1,3-dioxolane (DOL) polymerization that was initiated by cationic aluminum species. The *in situ* polymerized layer constitutes a conformal interface between cathodes and anodes, and it accelerates both the bulk and interfacial ion migration.

The artificial interfacial layer can also be realized by solution immersion. Yan *et al.* [46] built a compact dual-layered protective layer through the *ex situ* reaction of fluoroethylene carbonate (FEC) solvent with metallic Li (Figure 3(b)). The decomposed FEC structures and products were carefully probed through AIMD simulations and X-ray photoelectron spectroscopy (XPS) spectra, revealing a bi-layer structure with organic components (i.e., ROLi, $ROCO_2Li$) facing the nonaqueous electrolytes and inorganic layer (i.e., LiF, Li_2CO_3) on the metal surface. The protected Li-metal anode rendered stable performances in Li | NCM cells at 0.5 C.

In addition, because a sulfurized interface was comprehensively investigated regarding the effect of species on the polysulfide concentration [47,48], Zhang and co-workers [49] further proposed an *ex situ* electrochemical strategy to make an implantable SEI (Figure 3(c)), where the Li-metal was precycled in Li bis-trifluoromethanesulfonimide (LiTFSI)-$LiNO_3$-Li_2S_5 ternary-salt DOL/DME (DME=1,2-dimethoxyethane) electrolytes to form an ultra-stable surface as a SEI initiator. This *ex situ*-formed layer can be transformed and applied in other electrolyte systems, such as esters, offering continuous protection for Li-metal anodes

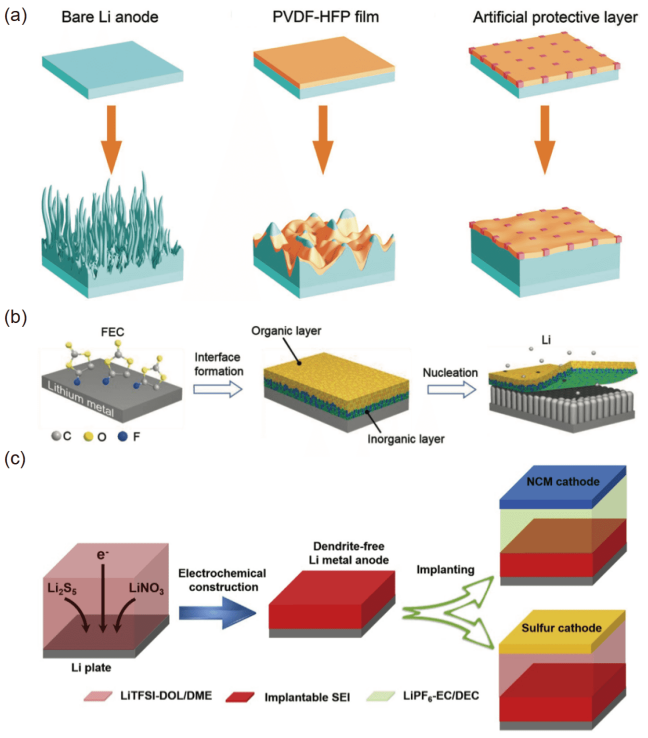

Figure 3 *Ex situ* formed interfacial layers. (a) Schematic illustrations of Li deposition without protection, lithium metal dendrites and dead Li forms after cycling; with a pure PVDF-HFP layer that is of poor mechanical modulus, interfacial fluctuation with dendrites piercing the PVDF-HFP layer occur after cycling; and with composite layer composed of organic PVDF-HFP and inorganic LiF that is conformal and mechanically strong to suppress Li dendrites penetration and stabilize Li metal surface [44]. (b) Schematic diagram of the dual-layered film formed on the Li-metal anode via FEC treatments. The organic and inorganic layers are achieved on the Li surface by spontaneous reactions between the Li-metal and FEC. The dual-layered film can regulate the uniform deposition of Li-ions during repeated charge/discharge cycles and protect the Li-metal anode without dendrite formation [46]. (c) Schematic of the *ex situ* SEI construction and morphology of the induced Li plate. *Ex situ* SEI construction on the Li plate by electrochemical methods in the 1.0 M LiTFSI-DOL/DME electrolyte with 0.020 M Li_2S_5-5.0 wt% $LiNO_3$ hybrid additives and its applications in Li-S and Li-NCM batteries [49] (color online).

and can be applied in both Li-S and Li-NCM batteries. Generally, constructing an interfacial layer alone cannot guarantee stable operation under a high current density. It is beneficial to combine a well-protected surface layer with structured current collectors to decrease the local current density and accommodate Li-metal anodes [50].

3.2 *In situ*-formed interfacial layer

3.2.1 In situ-formed interfacial layers induced by ion-solvent complexes

Theoretical investigations have revealed that ion-solvent complexes react with electrodes and constitute a significant part of the interfacial layer, where anions and solvents can be altered to adjust the solvation sheath [2,51].

In ion-solvent complexes, anion regulations provide an

effective route toward a stable and uniform interfacial layer. Among the various anions, it is rewarding to employ NO_3^- in electrolytes, which contributes much to the enhancement of cycling performances for practical Li batteries. The mechanism of lithium nitrate ($LiNO_3$) has been previously attributed to the unique physiochemical properties of the SEI and ion deposition behaviors. Zhang *et al*. [52] investigated the role of $LiNO_3$ from the view of the fundamental solvation state and interactions, where lithium bis(fluorosulfonyl) imide (LiFSI), $LiNO_3$, and DME were introduced as a model system to confirm the anion regulation concept. ^{17}O NMR, MD simulations, and XPS were used to determine the detailed interactions: NO_3^- anions help to polarize the solvation sheaths containing FSI^-, leading to activated anions and a complete FSI^- deposition in ether electrolytes with abundant $LiSO_x$, LiF, and LiN_xO_y on the Li-metal surface (Figure 4(a, b)). This phenomenon also induces a widened electrochemical stability window and aluminum current collector protection. In addition, electrolytes that replace $LiNO_3$ with $LiClO_4$ also exhibit similar features, confirming the generality of the anion interactions.

Solvents, as the other essential part in nonaqueous electrolytes, can also be modified to construct a desirable in situ-formed interfacial layer, among which fluorinated interphases are promising for dendrite-free Li battery operations [53]. Electrolyte additives, such as fluoroethylene carbonate (FEC), are beneficial for dense LiF interphase construction and have been confirmed to be effective on graphite [54,55], hard carbon [56], Li_xSi_y alloy [57], MoS_2-C anode [58], etc. Zhang *et al*. [59] introduced 5% FEC into commercial EC/diethyl carbonate (DEC) electrolytes. FEC is decomposed prior to the carbonate solvents on the Li-metal anodes owing to the lower LUMO energy level compared with EC and DEC, where the carbon-fluorine bond is broken from LiF, according to first-principles studies. LiF is regarded as a key SEI component for uniform Li deposition [60]. Upon sacrifice by FEC, the proportion of FEC increased from 29.5% in the EC/DEC electrolyte to 48.2%, which was induced by spontaneous reactions of FEC and metallic Li to prevent further reactions, rather than continuous EC/DEC consumption (Figure 4(c)). The FEC-protected anode exhibits a high specific capacity and long cycle life coupled with a high-loading $LiNi_{0.5}Co_{0.2}Mn_{0.3}O_2$ (NMC) cathode, and it exhibits practical application prospects.

Furthermore, the anions and solvents in solvation sheaths can be jointly mediated. Both lithium nitrate and FEC were used by Zhang and co-workers [51] to mediate the solvation of Li-ions (Figure 4(d, e)). MD simulations revealed that 30% of solvents become solvated with Li-ions in the FEC/$LiNO_3$ electrolyte. $LiNO_3$ participates in the solvation sheath and helps to generate LiN_xO_y on the anode surface. FEC acts as a major solvated solvent because the cyclic carbonate solvent is preferentially conscripted by Li-ions rather than its

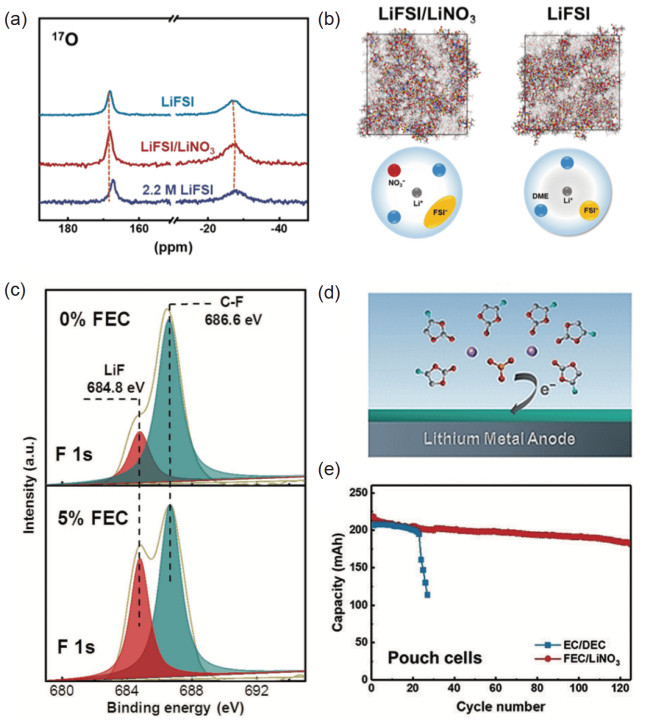

Figure 4 *In situ*-formed interfacial layers induced by ion-solvent complexes. (a) Natural abundance ^{17}O NMR spectra of LiFSI/$LiNO_3$ and related electrolytes measured at 50 °C. (b) Top panel: snapshots of the MD simulation boxes for the LiFSI/$LiNO_3$ and LiFSI electrolyte. Colors for different atoms: H-white, Li-purple, C-gray, O-red, N-blue, F-green, and S-yellow. The unsolvated solvents are in light gray. Bottom panel: schematics of the solvation structure of Li-ions in the corresponding electrolyte [52]. (c) XPS spectra of the SEI layer in 5% FEC electrolytes. F 1s spectra of the SEI layer induced by 0% and 5% FEC after Li stripping on a Cu substrate after ten cycles [59]. (d, e) The schematics of the solvation sheath of Li-ions and the SEI formed in FEC/$LiNO_3$ electrolytes in which PF_6^- is not shown for clear comparison. The cycling performance of Li|$LiFePO_4$ pouch cells with a theoretical capacity of 0.25 A h at 0.2 C after one cycle at 0.05 C. Here 50-mm-thick Li foils were used as the anodes [51] (color online).

linear counterpart [61]. Compared with routine EC/DEC electrolytes, the alternation of solvation sheaths leads to uniformly dispersed LiF and LiN_xO_y as decomposition products on the metal anodes. This *in situ*-formed interfacial layer provides a low-diffusion energy on the Li surface, a dendrite-free morphology, a prolonged cycle life, and has been applied in pouch cells.

3.2.2 *In situ-formed interfacial layers induced by electrolyte additives*

Electrolyte additives also contribute much to the SEI formation. By adjusting the synergy between the salt and solvent, even ether-based electrolytes can be stably cycled under high voltage, where the protective layer is constructed on both Li-metal anodes and cathodes [62,63]. Furthermore, even the electrochemical stability window of polyethylene oxide (PEO), a typical solid polymer electrolyte, can be considerably extended by introducing lithium bis(oxalato)

borate (LiBOB), $LiNO_3$, and halloysite nanoclay [64].

To construct a compact interfacial layer, Guo and co-workers [65] employed polyphosphoric acid (PPA) to react *in situ* with a primary SEI film and Li metal (Figure 5(a)). This Li_3PO_4 SEI layer remains stable during cycling without breakage in Li|$LiFePO_4$ battery systems. To achieve a higher stability and satisfying shape compliance, Li *et al.* [66] fabricated a smart layer on an Li-metal anode by an *in situ* reaction with polyacrylic acid (PAA) (Figure 5(b)), which was self-adapted, stable for 700 h of operation, and able to tolerate a huge deformation during repeated cycling according to *in situ* atomic force microscopy (AFM) characterizations.

Moreover, a controllable $AlCl_3$ additive and a trace amount of water can also be utilized for a stable and dendrite-free Li-metal anode (Figure 5(c)). The components of the formed interfacial layer have been carefully investigated, and interface reactions have been predicted. The feasibility of $AlCl_3$ additives have been demonstrated in Li|LTO and Li|selenium/microporous carbon (Se/MPC) full cells [67].

High-molecular weight polymers and ionic liquids can also act as additives in organic electrolytes. Wei *et al.* [68] dissolved poly(methyl methacrylate) (PMMA) in various solvents to form viscoelastic liquid electrolytes. They also proposed a power-law function of electrolyte viscosity and voltage window to further design the electrolytes. Consequently, reactive metals, including Li- and Na-metal, exhibit stable electrochemical deposition in these viscoelastic liquid electrolytes. Adding ionic liquids can also contribute to enhanced performances. Li *et al.* [69] passivated metallic Li through hybrid *N*-propyl-*N*-methylpyrrolidinium bis(triuoromethanesulfonyl)amide (Py13TFSI) and ether electrolytes. The synergy of ionic liquid and Li salt has been found to restrain Li corrosion during long operations. Li-metal|$LiFePO_4$ cells and Li|Li symmetric cells exhibit an enhanced stability and dendrite-free metal anode morphology.

4 Structural design of a solid electrolyte (SE)

With the increasing requirement of a high-energy density, safety concerns have become important, which have stimulated the search for high-performance solid-state Li-metal batteries (SLMBs) with SEs that are stable with both electrodes that exhibit a low interface resistance and can suppress the free growth of Li dendrites. In response to these requirements, various SEs have been explored, including inorganic ceramic electrolytes (ICEs) and solid polymer electrolytes (SPEs) [70]. However, an electrolyte without a special structure has its own drawbacks that cannot fulfill all the demands in SLMBs, regardless of the ICEs or SPEs. Therefore, structuring SEs can be an efficient strategy to elevate the performances of SLMBs. Many structures have been proposed, including an interpenetrating network structure, a double network structure, a porous interface structure, a sandwich structure, and a asymmetric structure, etc.

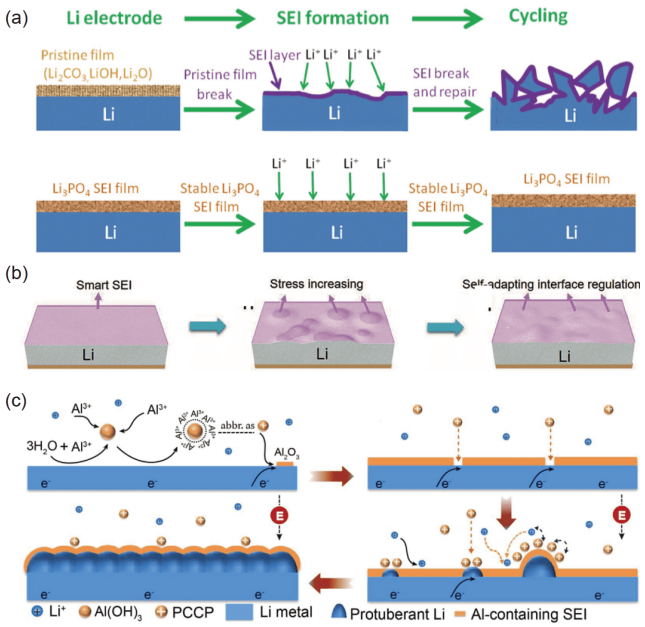

Figure 5 *In situ*-formed interfacial layers induced by electrolyte additives. (a) Schematics of the different Li anode structures. General Li-metal and Li_3PO_4-modified Li-metal anodes during SEI formation and cycling [65]. (b) The flexible PAA layer that decreases the Li dendrite growth by self-adapting interface regulation [66]. (c) Schematic diagrams showing the Li plating process in the electrolyte with the $AlCl_3$ additive [67] (color online).

4.1 Interpenetrating network and double network structure

SPEs that are easily prepared, have low cost, and are stable, have attracted extensive attention, but producing a SPE with a high ionic conductivity and high mechanical toughness simultaneously is still a big challenge. Many strategies have been proposed, such as comb-like polymer electrolytes [71,72], a random binary brush architecture [73], star-branched polymers [74], hierarchical nesting doll-like electrolytes [75], slide ring gel polymer electrolytes [76], and block/grafted copolymer electrolytes [77]. In block/grafted copolymer electrolytes, the block polymers are usually robust polymers that mainly assure that the mechanical strength of the electrolyte and the grafted polymers are flexible to aid the ions to move fast enough in the electrolyte. Synthesizing block/grafted copolymer electrolytes is an efficient way to obtain an electrolyte with satisfactory mechanical strength and a high ionic conductivity. However, the synthesizing methods for such copolymers are usually complicated, which may hinder mass production. Easier methods are anticipated for the preparation of more appropriate SPEs. Recently, Guo

et al. [78] proposed a simple method to acquire a bifunctional solid polymer electrolyte with an interpenetrating network in poly(ether-acrylate) (ipn-PEA) (Figure 6(a)). With a rigid interpenetrating network in the electrolyte, the copolymer electrolyte is able to resist the pressure, thus assuring its high mechanical strength (ca. 12 GPa), which may help restrain the Li dendrite and promote uniform Li plating/stripping. Moreover, the electrolyte network led to cages that could hold PEO molecules and restrain PEO crystallization; thus, the ipn-PEA electrolyte could maintain a high ionic conductivity (0.22 mS cm^{-1}) (Figure 6(b)). Another efficient method to obtain a desired SPE is to design a SPE with a double network in which the crystallization of each electrolyte is significantly reduced, thereby improving the ionic conductivity (Figure 6(c, d)) [79]. Overall, the double network structure can provide a high mechanical strength and thermal stability for the SPE. SLMBs with this double network SPE (DN-SPE) exhibited good stability with a Li-metal anode and a smooth morphology after cycling.

4.2 Porous interfacial structure

Garnet-type $Li_7La_3Zr_2O_{12}$ (LLZO) is one of the most promising candidates because of its high ionic conductivity (10^{-3} to 10^{-4} S/cm), strong mechanical stiffness, high Li^+ transfer number, and good stability against Li-metal [80,81]. However, LLZO is plagued by the poor physical contact at the electrode/electrolyte interface [82,83], which results in discontinuous Li^+ transfer. Li^+ transfer at the electrode/electrolyte interface is critical to obtain a stable electrochemical performance for SLMBs. To acquire a continuous conductive pathway of Li^+ transfer at the electrode/electrolyte interface, Rupp and co-workers [84] proposed a porous garnet-encapsulated electrode material (Figure 7(a)). As a result, the interface-engineered SLMBs exhibited improved charge/discharge capacities and cycling properties. When used in a Li-S solid battery, this porous structure acts as a host of cathode materials, which can significantly improve the sulfur cathode loading by more than 7 mg cm^{-2}, setting the barrier of a low mass loading in solid batteries (Figure 7(b)) [85]. Moreover, this porous structure can accommodate a volume change of the S cathode during the charge/discharge process, resulting in improved electrochemical performance (Figure 7(c)) [85]. In contrast to cathode materials, this porous structure can also mitigate the volume change of Li-metal during cycling and reduce the local current density of the Li anode, which significantly improves the working current density of the solid battery (Figure 7(d, e)) [74]. Consequently, the porous structure can increase the cathode mass loading, provide a continue Li^+ transfer pathway, accommodate a volume change, and reduce the local current density, which make the garnet electrolyte closer to commercialization [86].

4.3 Sandwich structure

Although ceramic electrolytes show many advantages, as mentioned above, the high electrode/electrolyte interfacial resistance has impeded its application in SLMBs. Moreover, the poor interface contact between Li and the ICE induces an uneven Li^+ flux and large overpotential on the Li/SE interface, which results in the growth of Li dendrites. Recent strategies to reduce the interfacial resistance of an ICE have mainly focused on introducing a polymer or gel between the

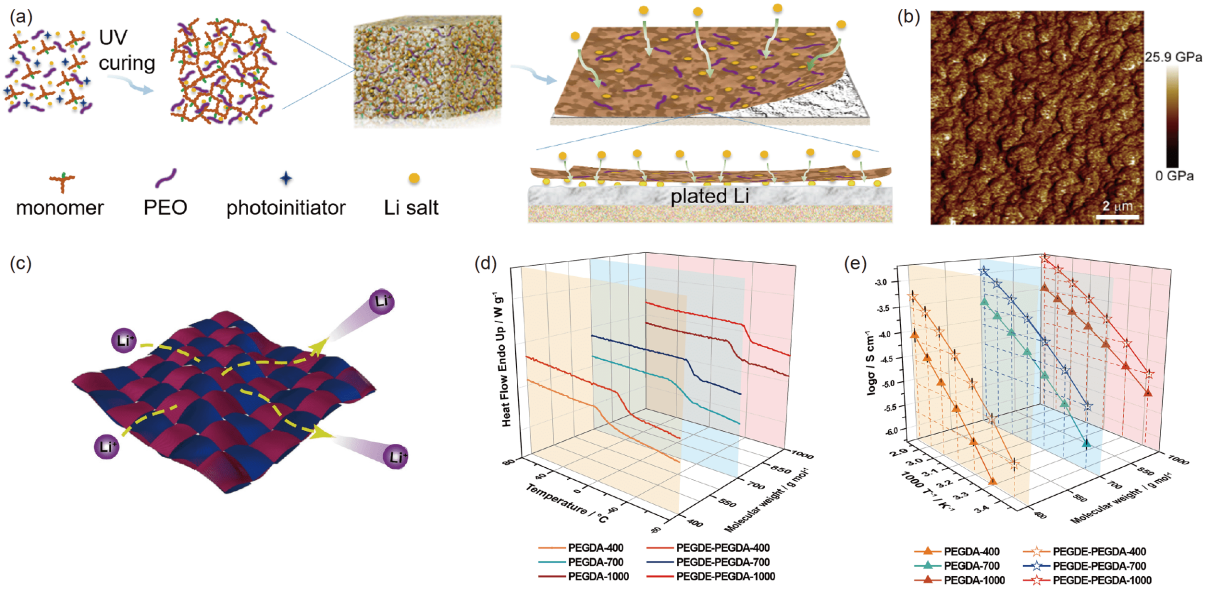

Figure 6 Interpenetrating network and double network structure. (a) Schematic diagram and (b) Young's modulus mapping of an ipn-PEA electrolyte [78]. (c) Schematic diagram, (d) DSC, and (e) ionic conductivity of DN-SPE [79] (color online).

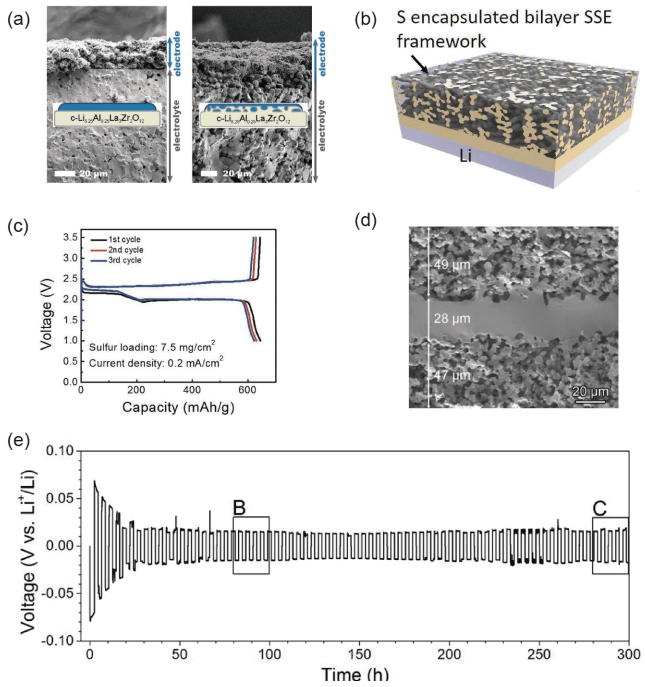

Figure 7 Porous structure of a solid electrolyte. (a) SEM images of sintered pellet cross-sections with composite nano-$Li_4Ti_5O_{12}$ electrodes for nonmodified (left) and interface-engineered (right) pellets [84]. (b) Schematic of a hybrid solid-state bilayer Li-S battery. (c) Voltage profile of the hybrid bilayer Li-S cell with a high sulfur mass loading of approximately 7.5 mg cm^{-2} at 0.2 mA cm^{-2} [85]. (d) Cross-sectional SEM image of the 3D garnet host. (e) Discharge/charge voltage profiles of the Li cycling in the garnet host at 0.5 mA cm^{-2} [74] (color online).

ICE and electrodes [87–89]. Goodenough and co-workers [90] reported a polymer/ceramic/polymer sandwich electrolyte (PCPSE), which integrated the advantage of an ICE and SPE. Of these, the SPE ensures a compact Li/SE interface and uniform Li^+ flux owing to the better wetting ability of the SPE on the Li anode, avoiding the direct contact of the ICE and Li anode. Additionally, an ICE can block the transfer of anions, facilitating stabilization of the SPE owing to the reduced electric field across the interface. As a result, SLMBs with this PCPSE have shown a high Coulombic efficiency of 99.8%−100% over 640 cycles.

4.4 Asymmetric structure

The required properties of a Li anode and cathode are inherently contradictory in SLMBs. From a mechanical point of view, the cathode prefers a flexible SE to build a compact cathode/SE interface. However, a Li anode requires a rigid SE to block the penetration of Li dendrites. From electrochemical stability point of view, the cathode requires a SE with a good oxidation resistance and that is compatible with high-voltage cathodes, and this would improve the energy density of a solid battery [91]. On the contrary, a Li-metal with a more negative equilibrium potential requires an SE with good reduction stability to match to Li anode. To fulfill the mutually contradictory requirement of the cathode and Li anode, Guo *et al*. [92] proposed an asymmetric structure for the SE that had specific aims. To solve the inconsistent mechanical issues, a rigid ceramic layer modified with an ultrathin polymer was employed to contact with the Li anode, inhibiting the free growth of Li dendrites, and a flexible SPE was introduced into the cathode through *in situ* thermal polymerization to obtain a simultaneously connected interface (Figure 8(a)). Furthermore, to achieve a high-voltage solid Li-metal battery, an oxidation-resistant poly(acrylonitrile) (PAN) was chosen on the cathode side that was compatible with Ni-rich cathodes. Meanwhile, polyethylene glycol diacrylate, which is reduction tolerant, was modified on the Li anode (Figure 8(b)). Consequently, the electrochemical window of SE was largely extended to 0–5 V (Figure 8(c)) [93]. Moreover, a Janus PAN@$Li_{1.4}Al_{0.4}Ge_{1.6}(PO_4)_3$ (80 wt%) composite electrolyte was introduced to suppress the penetration of Li dendrites and ensure a good interfacial contact [93]. Importantly, the total thickness of the structured SE was approximately 25 μm (Figure 8(b)). As a result, the assembled solid Li-metal battery that had this structured SE and Ni-rich cathodes, such as $LiNi_{0.6}Co_{0.2}Mn_{0.2}O_2$ (NCM622) and $LiNi_{0.8}Co_{0.1}Mn_{0.1}O_2$ (NCM811), exhibited a highly reversible capacity and long cycle life (Figure 8(d)). Excellent electrochemical performances for the SLMBs with the $LiCoO_2$ cathode were acquired through suitable assembly of an appropriate SPE [94]. These results indicate that an asymmetric structure is a good solution to fulfill the different demands for a solid battery and can extend the application of SEs.

5 Interfaces associated with a SE in Li-metal solid-state batteries

Li-metal solid-state battery, with high-energy density and safety, has been considered potential for future consumer electronics and electronic vehicles. However, the key issue of solid-solid interfaces in solid-state battery is urged to be addressed. The solid-solid interfaces generally involve physical contact and chemical contact [95]. Although the physical contact issue can be much alleviated by operating batteries at the temperature above the Li-metal melting point for grid energy storage [96], the point-to-point contact of batteries operated under room temperature leads to poor electron and ion transport. The obstacle of limited physical contact includes volume change of electrode particles and inorganic electrolyte during charge-discharge cycles. Chemical contact indicates side reactions at interfaces in batteries, resulting in high interfacial resistance and instability. Besides, it also leads to the formation of a SEI that can modify the interfaces in batteries.

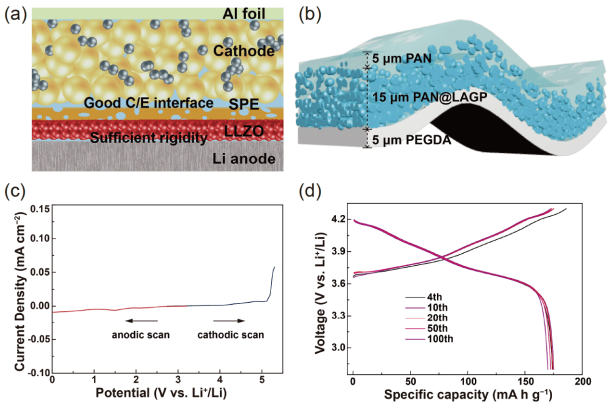

Figure 8 Asymmetric solid electrolyte. Schematic of SEs to overcome the inconsistent (a) mechanical [92] and (b) electrochemical stability issues. (c) Electrochemical window of the SE was expended to 0–5 V. (d) Electrochemical performance of SLMBs with the structured SE and NCM811 cathode [93] (color online).

Herein, interfaces associated with SE in Li-metal solid-state batteries are discussed in two major aspects, SE-Li anode interface and hybrid SE internal interface.

5.1 Interface between the SE and the Li-metal anode

To improve the interface stabilities toward the Li-metal anode, gel polymer electrolytes (GPEs) have received extensive interest for their superior stabilities compared with traditional liquid electrolyte [97,98]. *In situ* polymerization of GPE is an effective approach to solve the interfacial contact problems in integrated batteries [99]. However, most of the present strategies of *in situ* polymerization require the presence of initiators and special conditions, such as high temperature, which is harmful for the stable Li/electrolyte interface. Recently, Li *et al*. [100] proposed a cationic ring-opening polymerization between $LiPF_6$ and DOL in commercial ether-based electrolyte that converts a traditional liquid electrolyte into a GPE without any impurities at room temperature (Figure 9(a)). Importantly, although originating from a conventional electrolyte, the GPE displays superior compatibility with a Li-metal anode and exhibits remarkably stable Li deposition and dissolution behaviors. In a Li-S battery, this GPE exhibit efficacious restriction of polysulfide diffusion (Figure 9(b)). The electrochemical stability interval is significantly broadened to match the NCM622 cathode.

Compared with the cathode-SE interface, physical contact on the interface between a Li-metal anode and an SE is not that critical because of the ductility of the Li-metal. The interfacial resistance of the SE and Li-metal is strongly related to the adhesion strength [101]. Instead, Li dendrite growth is a long-standing problem for the Li anode. For inorganic electrolytes, although they have sufficient modulus to suppress Li dendrite growth, the Li-metal infiltrates at the defects above a critical current density. Porz *et al*. [102] verified that Li penetration depends on pre-existing flaws, defect size, and density, rather than shear modulus. Therefore, introducing a buffer layer has been proposed to sufficiently alleviate the interfacial problem between the Li anode and inorganic electrolyte. For example, a fluorinated SE interphase was proposed to be *in situ*-formed on Li_3PS_4 to suppress Li dendrite growth (Figure 9(c)) [53]. The LiF-enriched SEI contributes to a high critical current density (>2 mA cm^{-2}) and superior Li plating/stripping cycling performance. Moreover, Chen *et al*. [103] introduced a Li_2S buffer layer between the Li anode and the Li_6PS_5Cl SE. A stable interface system was established at the atomic level by preventing the destruction of the PS_4 tetrahedral structure. Diffusion of S and Cl atoms from LPSCl to the Li-metal anode was inhibited by the buffer layer, and no Li adsorption sites were observed at the Li/Li_2S interface, which suggests that Li_2S effectively provides a smooth interface structure.

Regarding the solid polymer electrolyte, Li dendrites grow at all current densities and a consequential unstable morphology for the interface between Li and the polymer is a substantial hindrance [104,105]. Therefore, including improving the mechanical strength and ionic conductivity, designing a SE interphase between Li and the polymer is also effective for meeting the challenge of the interface between the polymer electrolyte and the Li-metal anode. Guo *et al*. [106] constructed a Li anode safeguard composed of Al-containing (oxy)fluorides (Figure 9(d)), which was *in situ*-fabricated by lithiation of nanosized $AlPO_4$. The repellent in infiltrated quasi-SE can ameliorate the interfacial stability by ensuring a uniform Li deposition and promoting the cycle performance of solid batteries. Another design strategy for quasi-SEs for Li-metal anodes is to host liquid electrolytes in the pores of a cross-linked polymer network for stable electrodeposition. Choudhury *et al*. [107] proposed free-standing structured electrolytes with polymer-grafted nanoparticles in which the pore sizes can be manipulated by changing the nanoparticle volume fraction.

Furthermore, designing an anion-immobilized SE is also an effective strategy to induce homogeneous deposition of Li-ions. Zhang and co-workers [108] proposed the linking of anions onto a polymer matrix (PEO) and ceramic fillers (LLZTO) via dispersion (Figure 9(e)). In this method, free Li cations can transport uniformly and rapidly, which results in continuously dendrite-free plating on the metallic Li anode that is driven by the electrical field.

5.2 Interface between different components in a hybrid SE

Because a single-component SE cannot currently meet the different requirements of Li-metal all-solid-state batteries, integrating a solid polymer with an inorganic electrolyte is of

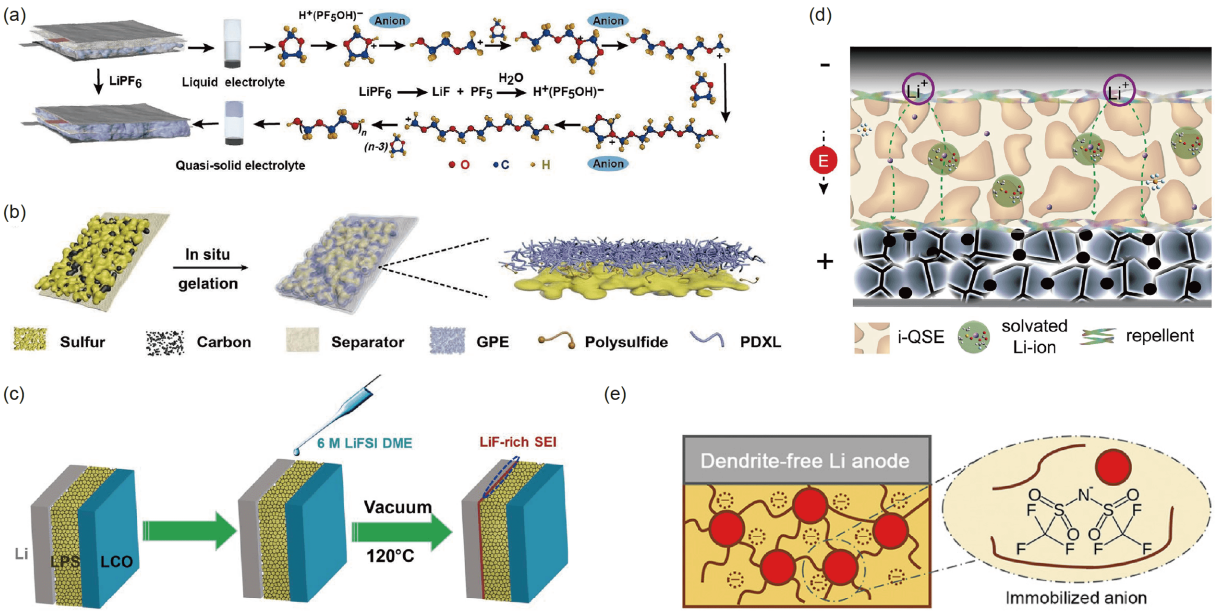

Figure 9 SE/Li-metal anode interface. (a) Schematic model of the polymerization mechanism of DOL induced by $LiPF_6$. (b) Schematic diagram of the *in situ* polymerization inside the Li-S battery system [100]. (c) Schematic of the *in situ* preparation of the fluorinated SE interphase between the Li-metal anode and LPS SE. The optimized structures of the three interface structures [53]. (d) Schematic of different interface structures in the Li|i-QSE|LFP battery, including the repellent layer between the Li anode and i-QSE [106]. (e) Schematic illustrating the immobilized anions tethered to ceramic particles and polymer chains for achieving a dendrite-free Li anode [108] (color online).

interest. Thus, a hybrid SE internal interface is a key idea. Simply stacking different kinds of electrolytes or blending is clearly not a wise strategy. Research on the internal interface and interaction between the compositions of a hybrid SE has been carefully performed to investigate the basic characteristics of a hybrid SE.

To clarify the understanding of the interplay of a hybrid SE, Zheng *et al.* [109] employed NMR to study the Li^+ transport pathway in polymer-ceramic composite electrolytes (PEO-LLZO). The investigation showed that as the fraction of the LLZO phase increased, the Li-ion pathway transitioned from a polymer (PEO) to ceramic (LLZO) phase (Figure 10(a)). For the LLZO (20 wt%)-PEO (LiTFSI) composite, the decomposed LLZO phase serves as an additional Li source, and the PEO matrix is mainly for conduction. With the increase in LLZO content to 50 wt%, the LLZO and PEO-LLZO interface resonance began to show ^{6}Lienrichment. This showed that LLZO (50 wt%) forms a percolated network for major Li-ion transportation, and PEO (LiTFSI) also undertakes a small portion, whereas the decomposed LLZO phase plays a minor role. Clearly, for the LLZO (50 wt%)-PEO ($LiClO_4$) composite electrolyte, few Li^+ prefer to travel through the PEO matrix, which is affected by the type of Li salt (Figure 10(b)) [110]. Yang's group also explored the PAN-LLZO composite SE (Figure 10(c)) [111]. Unlike the PEO-LLZO composite electrolyte, their research reveals that Li-ions prefer to transport through the interface between the LLZO and PAN phase, which is a LLZO-modified PAN phase. The above-mentioned hybrid SEs exhibit considerable Li ionic conductivity, which was determined by the ion mobility, active ion concentration, and transport pathway. A deep investigation of the interfaces in the composite electrolyte would be beneficial to study the interaction between the compositions and to improve its ionic conductivity.

Moreover, Zhang *et al.* [112,113] presented synergistic coupling between LLZTO and PVDF, which not only highly enhanced the mechanical strength but also the ionic conductivity. LLZTO complexed with solvent molecules to induce the dehydrofluorination of the PVDF, which further modified the interface between LLZTO and PVDF (Figure 10(d)). This influenced the interplay between the ceramic fillers, polymer matrix, and Li salt, which affected the transport pathways of Li-ions and further electrochemical parameters. The LLZTO-based PVDF composite electrolyte displays an excellent ionic conductivity at room temperature, which is promising for all-solid-state Li batteries. Moreover, interfaces also exist within polycrystalline ceramic electrolytes, where ions migrate through intergranular paths (between grains), intragranular paths (inside grains), and paths within the grain boundary. Additionally the grain boundary conductivities have been varied with the operational temperature [114]. Weppner and co-workers [114] estimated that the grain boundary resistance contributions 40%–50% to the total resistance of $Li_7La_3Zr_2O_{12}$ (LLZO).

Hence, the interplay of a composite SE deserves more understanding. It is possible to observe and regulate the interactions between integrated multi-components of an SE to

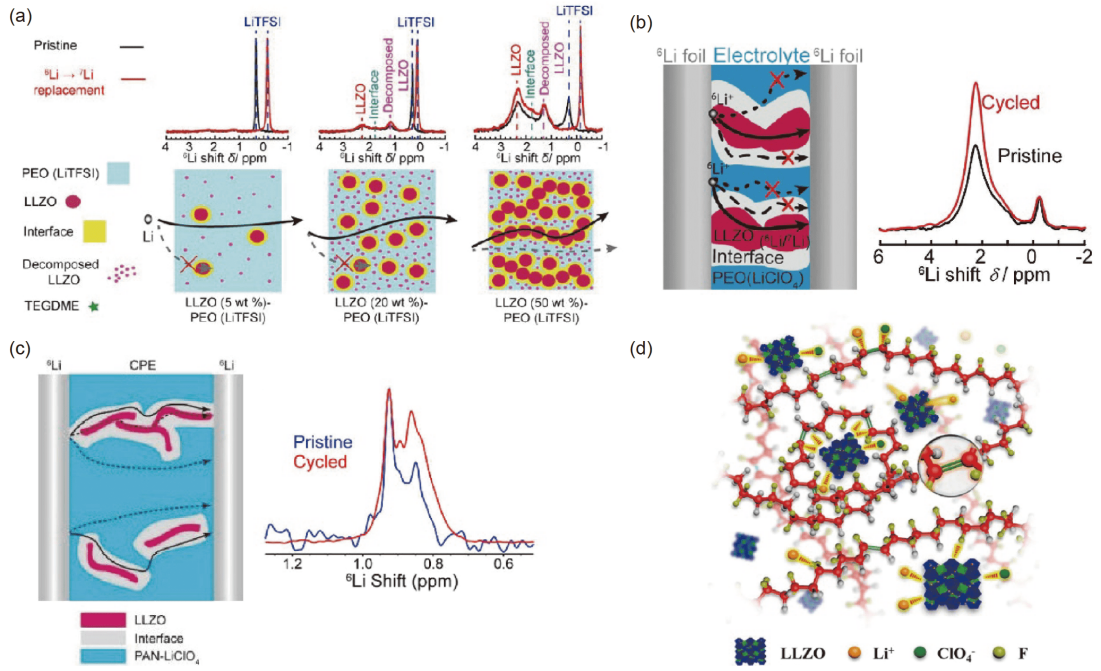

Figure 10 ^{6}Li NMR comparison of pristine and cycled composite electrolytes and a schematic of the possible Li^{+} transport pathways. (a) LLZO-PEO (LiTFSI) with different fractions of LLZO [109], (b) LLZO-PEO ($LiClO_4$) [110], and (c) LLZO-PAN ($LiClO_4$) [111]. (d) Possible complex structures of the LLZTO-based PVDF composite electrolyte at the molecular level [112] (color online).

achieve practical Li-metal batteries.

6 Conclusions and perspective

Rechargeable Li-metal batteries have been strongly considered as promising candidates in next-generation energy storage devices for portable electronics and electric vehicles and can be potentially applied in stationary electricity storage. The high reactivity and decreased density of the metallic Li anode result in not only a fantastic energy density but also an inevitable interface layer on the surface between the Li anode and electrolytes. Multiple advanced techniques have been applied to understand the process that fundamentally occurs at the interface, and the development of nanoscience and nanotechnology provides abundant opportunities to regulate the interface structure and components effectively.

Theoretical calculations and model experiments have confirmed that Li ions exist as ion-solvent complexes in nonaqueous electrolytes, whose solvation structures considerably determine the interfacial composition. The various components in the interface layer exhibit different ion and electron conduction abilities. A mixed conductive layer constitutes a transition state of a SEI or an inner layer of a stable interfacial film. Moreover, a solid-state Li ionic conductor can also act as an artificial interface for Li-metal anodes. The design of solid-state electrolytes, including interpenetrating networks, double networks, porous interfaces, sandwiches, and asymmetric structures, has been quite successful, where Li-ion transportation through interfaces inside hybrid SEs and SE/Li-metals is also considerably enhanced. Importantly, many of these strategies have been demonstrated in pouch cells for further practical applications. The strategies in liquid electrolytes, such as introducing various additives, will achieve the most rapid growth because they integrate most easily into existing techniques. To further achieve the goal of a high energy density, high safety, and long cycle life, the evolution from nonaqueous to gel, half-solid, and solid-state batteries is predicted because the energy storage capability and balanced performances will not be suddenly enhanced according to history. Various strategies will be further developed and applied for different battery systems at different stages.

Despite the notable progresses above, there is still a large open space for interface science and engineering in the development of high-energy-density, long-lived, and safe Li-metal batteries. (1) Of note, publishing a single perfect result does not guarantee that the battery can be practically applied. The electrolyte quantity, active material loading of the electrodes, N/P ratio, cell fabrication, and testing protocol are all sensitive to the obtained cycling performance, which is crucial for both large-format cells and coin cells [115]. (2) The ability to construct high-capacity, large-format batteries that are able to cycle at a high current density, high capacity and high utilization of the Li metal anode is necessary for

commercialization. (3) Furthermore, the compatibility of cathodes is another barrier to achieve a practical Li-metal battery, especially when operated at a high voltage for increased energy density. (4) To go beyond the horizon of current batteries, advanced characterizations, especially *in situ* and operando techniques, make it possible to track the material evolution process in working batteries and determine the factors required to diminish the capacity, thus offering considerable inspiration for interface design. (5) Moreover, scientific computing combined with nanoscience will considerably accelerate the discovery of novel functional materials and the chemistry principles behind these interrelated performances. Although there are still deviations between calculated and experimental results, high-throughput screening also helps us reject compounds and narrow the scope. There are abundant challenges and opportunities in this field. Only through close cooperation between chemistry, materials, and engineering fields can we obtain innovations to realize the ultrahigh energy storage offered by Li-metal chemistry.

Acknowledgements This work was supported by the National Key Research and Development Program (2016YFA0202500, 2016YFA0200102), the National Natural Science Foundation of China (21676160, 21825501, 21773264, 21805062, U1801257), Beijing Natural Science Foundation (L172023), and Tsinghua University Initiative Scientific Research Program.

Conflict of interest The authors declare that they have no conflict of interest.

1 Cheng XB, Zhang R, Zhao CZ, Zhang Q. *Chem Rev*, 2017, 117: 10403–10473
2 Chen X, Hou T, Persson KA, Zhang Q. *Mater Today*, 2019, 22: 142–158
3 Xin S, Chang Z, Zhang X, Guo YG. *Nat Sci Rev*, 2017, 4: 54–70
4 Chen S, Niu C, Lee H, Li Q, Yu L, Xu W, Zhang JG, Dufek EJ, Whittingham MS, Meng S, Xiao J, Liu J. *Joule*, 2019, 3: 1094–1105
5 Zhang XQ, Zhao CZ, Huang JQ, Zhang Q. *Engineering*, 2018, 4: 831–847
6 Sun YZ, Huang JQ, Zhao CZ, Zhang Q. *Sci China Chem*, 2017, 60: 1508–1526
7 Li NW, Yin YX, Xin S, Li JY, Guo YG. *Small Methods*, 2017, 1: 1700094
8 Ye H, Xin S, Yin YX, Guo YG. *Adv Energy Mater*, 2017, 7: 1700530
9 Lu Y, Zhang Q, Chen J. *Sci China Chem*, 2019, 62: 533–548
10 Duan H, Zhang J, Chen X, Zhang XD, Li JY, Huang LB, Zhang X, Shi JL, Yin YX, Zhang Q, Guo YG, Jiang L, Wan LJ. *J Am Chem Soc*, 2018, 140: 18051–18057
11 Cheng XB, Zhao CZ, Yao YX, Liu H, Zhang Q. *Chem*, 2019, 5: 74–96
12 Li BQ, Chen XR, Chen X, Zhao CX, Zhang R, Cheng XB, Zhang Q. *Research*, 2019, 2019(2): 4608940
13 Guo YG, Chen J. *Sci China Chem*, 2017, 60: 1481–1482
14 Xu X, Wang S, Wang H, Hu C, Jin Y, Liu J, Yan H. *J Energy Chem*, 2018, 27: 513–527
15 Li L, Chen C, Yu A. *Sci China Chem*, 2017, 60: 1402–1412
16 Li Y, Li Y, Pei A, Yan K, Sun Y, Wu CL, Joubert LM, Chin R, Koh AL, Yu Y, Perrino J, Butz B, Chu S, Cui Y. *Science*, 2017, 358: 506–510
17 Bieker G, Winter M, Bieker P. *Phys Chem Chem Phys*, 2015, 17: 8670–8679
18 Cheng H, Zhu CB, Lu M, Yang Y. *J Power Sources*, 2007, 174: 1027–1031
19 Sacci RL, Black JM, Balke N, Dudney NJ, More KL, Unocic RR. *Nano Lett*, 2015, 15: 2011–2018
20 Kanamura K, Tamura H, Shiraishi S, Takehara Z-i. *J Electrochem Soc*, 1995, 142: 340–347
21 Aurbach D, Weissman I, Zaban A, Chusid O. *Electrochim Acta*, 1994, 39: 51–71
22 Aurbach D. *J Power Sources*, 2000, 89: 206–218
23 Cheng XB, Zhang R, Zhao CZ, Wei F, Zhang JG, Zhang Q. *Adv Sci*, 2016, 3: 1500213
24 Peled E, Golodnitsky D, Ardel G. *J Electrochem Soc*, 1997, 144: L208–L210
25 Malmgren S, Ciosek K, Hahlin M, Gustafsson T, Gorgoi M, Rensmo H, Edström K. *Electrochim Acta*, 2013, 97: 23–32
26 Cheng XB, Yan C, Zhang XQ, Liu H, Zhang Q. *ACS Energy Lett*, 2018, 3: 1564–1570
27 Maier J. *Solid State Ion*, 1995, 75: 139–145
28 Wenzel S, Randau S, Leichtweiß T, Weber DA, Sann J, Zeier WG, Janek J. *Chem Mater*, 2016, 28: 2400–2407
29 Shen X, Cheng X, Shi P, Huang J, Zhang X, Yan C, Li T, Zhang Q. *J Energy Chem*, 2019, 37: 29–34
30 Xue Y, Li Y, Zhang J, Liu Z, Zhao Y. *Sci China Chem*, 2018, 61: 765–786
31 Yan C, Cheng XB, Yao YX, Shen X, Li BQ, Li WJ, Zhang R, Huang JQ, Li H, Zhang Q. *Adv Mater*, 2018, 30: 1804461
32 Xu R, Sun Y, Wang Y, Huang J, Zhang Q. *Chin Chem Lett*, 2017, 28: 2235–2238
33 Nolan AM, Zhu Y, He X, Bai Q, Mo Y. *Joule*, 2018, 2: 2016–2046
34 Chen X, Shen X, Li B, Peng HJ, Cheng XB, Li BQ, Zhang XQ, Huang JQ, Zhang Q. *Angew Chem Int Ed*, 2018, 57: 734–737
35 Chen X, Hou TZ, Li B, Yan C, Zhu L, Guan C, Cheng XB, Peng HJ, Huang JQ, Zhang Q. *Energy Storage Mater*, 2017, 8: 194–201
36 Chen X, Li H-, Shen X, Zhang Q. *Angew Chem*, 2018, 130: 16885–16889
37 Chen X, Zhang XQ, Li HR, Zhang Q. *Batteries Supercaps*, 2019, 2: 128–131
38 Yan C, Yao YX, Chen X, Cheng XB, Zhang XQ, Huang JQ, Zhang Q. *Angew Chem*, 2018, 130: 14251–14255
39 Cui J, Zhan TG, Zhang KD, Chen D. *Chin Chem Lett*, 2017, 28: 2171–2179
40 Zhang XQ, Chen X, Xu R, Cheng XB, Peng HJ, Zhang R, Huang JQ, Zhang Q. *Angew Chem Int Ed*, 2017, 56: 14207–14211
41 Cheng XB, Zhao MQ, Chen C, Pentecost A, Maleski K, Mathis T, Zhang XQ, Zhang Q, Jiang J, Gogotsi Y. *Nat Commun*, 2017, 8: 336
42 Gao Y, Yan Z, Gray JL, He X, Wang D, Chen T, Huang Q, Li YC, Wang H, Kim SH, Mallouk TE, Wang D. *Nat Mater*, 2019, 18: 384–389
43 Zhao Q, Tu Z, Wei S, Zhang K, Choudhury S, Liu X, Archer LA. *Angew Chem Int Ed*, 2018, 57: 992–996
44 Xu R, Zhang XQ, Cheng XB, Peng HJ, Zhao CZ, Yan C, Huang JQ. *Adv Funct Mater*, 2018, 28: 1705838
45 Zhao Q, Liu X, Stalin S, Khan K, Archer LA. *Nat Energy*, 2019, 4: 365–373
46 Yan C, Cheng XB, Tian Y, Chen X, Zhang XQ, Li WJ, Huang JQ, Zhang Q. *Adv Mater*, 2018, 30: 1707629
47 Cheng XB, Yan C, Peng HJ, Huang JQ, Yang ST, Zhang Q. *Energy Storage Mater*, 2018, 10: 199–205
48 Zhao CZ, Cheng XB, Zhang R, Peng HJ, Huang JQ, Ran R, Huang ZH, Wei F, Zhang Q. *Energy Storage Mater*, 2016, 3: 77–84
49 Cheng XB, Yan C, Chen X, Guan C, Huang JQ, Peng HJ, Zhang R, Yang ST, Zhang Q. *Chem*, 2017, 2: 258–270
50 Zhang R, Chen X, Shen X, Zhang XQ, Chen XR, Cheng XB, Yan C, Zhao CZ, Zhang Q. *Joule*, 2018, 2: 764–777
51 Zhang XQ, Chen X, Cheng XB, Li BQ, Shen X, Yan C, Huang JQ,

Zhang Q. *Angew Chem Int Ed*, 2018, 57: 5301–5305
52 Zhang XQ, Chen X, Hou LP, Li BQ, Cheng XB, Huang JQ, Zhang Q. *ACS Energy Lett*, 2019, 4: 411–416
53 Fan X, Ji X, Han F, Yue J, Chen J, Chen L, Deng T, Jiang J, Wang C. *Sci Adv*, 2018, 4: eaau9245
54 Wang DY, Sinha NN, Burns JC, Aiken CP, Petibon R, Dahn JR. *J Electrochem Soc*, 2014, 161: A467–A472
55 Nie M, Demeaux J, Young BT, Heskett DR, Chen Y, Bose A, Woicik JC, Lucht BL. *J Electrochem Soc*, 2015, 162: A7008–A7014
56 Kohl M, Borrmann F, Althues H, Kaskel S. *Adv Energy Mater*, 2016, 6: 1502185
57 Shkrob IA, Wishart JF, Abraham DP. *J Phys Chem C*, 2015, 119: 14954–14964
58 Wang J, Luo C, Gao T, Langrock A, Mignerey AC, Wang C. *Small*, 2015, 11: 473–481
59 Zhang XQ, Cheng XB, Chen X, Yan C, Zhang Q. *Adv Funct Mater*, 2017, 27: 1605989
60 Lu Y, Tu Z, Archer LA. *Nat Mater*, 2014, 13: 961–969
61 von Wald Cresce A, Borodin O, Xu K. *J Phys Chem C*, 2012, 116: 26111–26117
62 Jiao S, Ren X, Cao R, Engelhard MH, Liu Y, Hu D, Mei D, Zheng J, Zhao W, Li Q, Liu N, Adams BD, Ma C, Liu J, Zhang JG, Xu W. *Nat Energy*, 2018, 3: 739–746
63 Ren X, Zou L, Jiao S, Mei D, Engelhard MH, Li Q, Lee H, Niu C, Adams BD, Wang C, Liu J, Zhang JG, Xu W. *ACS Energy Lett*, 2019, 4: 896–902
64 Zhao Q, Chen P, Li S, Liu X, Archer LA. *J Mater Chem A*, 2019, 7: 7823–7830
65 Li NW, Yin YX, Yang CP, Guo YG. *Adv Mater*, 2016, 28: 1853–1858
66 Li NW, Shi Y, Yin YX, Zeng XX, Li JY, Li CJ, Wan LJ, Wen R, Guo YG. *Angew Chem Int Ed*, 2018, 57: 1505–1509
67 Ye H, Yin YX, Zhang SF, Shi Y, Liu L, Zeng XX, Wen R, Guo YG, Wan LJ. *Nano Energy*, 2017, 36: 411–417
68 Wei S, Cheng Z, Nath P, Tikekar MD, Li G, Archer LA. *Sci Adv*, 2018, 4: eaao6243
69 Li NW, Yin YX, Li JY, Zhang CH, Guo YG. *Adv Sci*, 2017, 4: 1600400
70 Zheng Q, Yi H, Li X, Zhang H. *J Energy Chem*, 2018, 27: 1597–1617
71 Ji X, Zeng H, Gong X, Tsai F, Jiang T, Li RKY, Shi H, Luan S, Shi D. *J Mater Chem A*, 2017, 5: 24444–24452
72 Wang Y, Zhang Y, Hou H. *J Appl Electrochem*, 2017, 47: 237–248
73 Lyu YF, Zhang ZJ, Liu C, Geng Z, Gao LC, Chen Q. *Chin J Polym Sci*, 2018, 36: 78–84
74 Yang C, Zhang L, Liu B, Xu S, Hamann T, McOwen D, Dai J, Luo W, Gong Y, Wachsman ED, Hu L. *Proc Natl Acad Sci USA*, 2018, 115: 3770–3775
75 Zhou D, Liu R, Zhang J, Qi X, He YB, Li B, Yang QH, Hu YS, Kang F. *Nano Energy*, 2017, 33: 45–54
76 Sugihara N, Nishimura K, Nishino H, Kanehashi S, Mayumi K, Tominaga Y, Shimomura T, Ito K. *Electrochim Acta*, 2017, 229: 166–172
77 Paranjape N, Mandadapu PC, Wu G, Lin H. *Polymer*, 2017, 111: 1–8
78 Zeng XX, Yin YX, Li NW, Du WC, Guo YG, Wan LJ. *J Am Chem Soc*, 2016, 138: 15825–15828
79 Duan H, Yin YX, Zeng XX, Li JY, Shi JL, Shi Y, Wen R, Guo YG, Wan LJ. *Energy Storage Mater*, 2018, 10: 85–91
80 Zhu Y, He X, Mo Y. *ACS Appl Mater Interfaces*, 2015, 7: 23685–23693
81 Thangadurai V, Narayanan S, Pinzaru D. *Chem Soc Rev*, 2014, 43: 4714–4727
82 Xin S, You Y, Wang S, Gao HC, Yin YX, Guo YG. *ACS Energy Lett*, 2017, 2: 1385–1394
83 Canepa P, Dawson JA, Sai Gautam G, Statham JM, Parker SC, Islam MS. *Chem Mater*, 2018, 30: 3019–3027
84 van den Broek J, Afyon S, Rupp JLM. *Adv Energy Mater*, 2016, 6: 1600736
85 Fu KK, Gong Y, Hitz GT, McOwen DW, Li Y, Xu S, Wen Y, Zhang L, Wang C, Pastel G, Dai J, Liu B, Xie H, Yao Y, Wachsman ED, Hu L. *Energy Environ Sci*, 2017, 10: 1568–1575
86 Zhang XD, Shi JL, Liang JY, Yin YX, Guo YG, Wan LJ. *Sci China Chem*, 2017, 60: 1554–1560
87 Liu B, Gong Y, Fu K, Han X, Yao Y, Pastel G, Yang C, Xie H, Wachsman ED, Hu L. *ACS Appl Mater Interfaces*, 2017, 9: 18809–18815
88 Chinnam PR, Wunder SL. *ACS Energy Lett*, 2017, 2: 134–138
89 Wang Q, Wen Z, Jin J, Guo J, Huang X, Yang J, Chen C. *Chem Commun*, 2016, 52: 1637–1640
90 Zhou W, Wang S, Li Y, Xin S, Manthiram A, Goodenough JB. *J Am Chem Soc*, 2016, 138: 9385–9388
91 Zhao E, Yu X, Wang F, Li H. *Sci China Chem*, 2017, 60: 1483–1493
92 Duan H, Yin YX, Shi Y, Wang PF, Zhang XD, Yang CP, Shi JL, Wen R, Guo YG, Wan LJ. *J Am Chem Soc*, 2018, 140: 82–85
93 Duan H, Fan M, Chen WP, Li JY, Wang PF, Wang WP, Shi JL, Yin YX, Wan LJ, Guo YG. *Adv Mater*, 2018, 31: 1807789
94 Zhou W, Wang Z, Pu Y, Li Y, Xin S, Li X, Chen J, Goodenough JB. *Adv Mater*, 2019, 31: 1805574
95 Xu L, Tang S, Cheng Y, Wang K, Liang J, Liu C, Cao YC, Wei F, Mai L. *Joule*, 2018, 2: 1991–2015
96 Jin Y, Liu K, Lang J, Zhuo D, Huang Z, Wang C, Wu H, Cui Y. *Nat Energy*, 2018, 3: 732–738
97 Zhu M, Wu J, Wang Y, Song M, Long L, Siyal SH, Yang X, Sui G. *J Energy Chem*, 2019, 37: 126–142
98 Liu J, Zhang L, Li H, Zhao P, Ren P, Shi W, Cheng P. *Sci China Chem*, 2019, 62: 602–608
99 Zhang J, Yuan T, Wan H, Qian J, Ai X, Yang H, Cao Y. *Sci China Chem*, 2017, 60: 1546–1553
100 Liu FQ, Wang WP, Yin YX, Zhang SF, Shi JL, Wang L, Zhang XD, Zheng Y, Zhou JJ, Li L, Guo YG. *Sci Adv*, 2018, 4: eaat5383
101 Liu Q, Geng Z, Han C, Fu Y, Li S, He Y, Kang F, Li B. *J Power Sources*, 2018, 389: 120–134
102 Porz L, Swamy T, Sheldon BW, Rettenwander D, Frömling T, Thaman HL, Berendts S, Uecker R, Carter WC, Chiang YM. *Adv Energy Mater*, 2017, 7: 1701003
103 Chen B, Xu C, Wang H, Zhou J. *Curr Appl Phys*, 2019, 19: 149–154
104 Monroe C, Newman J. *J Electrochem Soc*, 2004, 151: A880
105 Monroe C, Newman J. *J Electrochem Soc*, 2005, 152: A396
106 Zeng XX, Yin YX, Shi Y, Zhang XD, Yao HR, Wen R, Wu XW, Guo YG. *Chem*, 2018, 4: 298–307
107 Choudhury S, Vu D, Warren A, Tikekar MD, Tu Z, Archer LA. *Proc Natl Acad Sci USA*, 2018, 115: 6620–6625
108 Zhao CZ, Zhang XQ, Cheng XB, Zhang R, Xu R, Chen PY, Peng HJ, Huang JQ, Zhang Q. *Proc Natl Acad Sci USA*, 2017, 114: 11069–11074
109 Zheng J, Hu YY. *ACS Appl Mater Interfaces*, 2018, 10: 4113–4120
110 Zheng J, Tang M, Hu YY. *Angew Chem Int Ed*, 2016, 55: 12538–12542
111 Yang T, Zheng J, Cheng Q, Hu YY, Chan CK. *ACS Appl Mater Interfaces*, 2017, 9: 21773–21780
112 Zhang X, Liu T, Zhang S, Huang X, Xu B, Lin Y, Xu B, Li L, Nan CW, Shen Y. *J Am Chem Soc*, 2017, 139: 13779–13785
113 Zhang X, Wang S, Xue C, Xin C, Lin Y, Shen Y, Li L, Nan CW. *Adv Mater*, 2019, 31: 1806082
114 Murugan R, Thangadurai V, Weppner W. *Angew Chem Int Ed*, 2007, 46: 7778–7781
115 Li H. *Joule*, 2019, 3: 911–914